Vol. 25, No. 2(2026) IA26791
Revista Mexicana de Ingeniería Química

Aluminum – modified rice husk biochar for effective fluoride adsorption

Biochar de cáscara de arroz modificado con aluminio para una efectiva adsorción de fluoruro

G.X. Martinez-Paredes*, L. Lopez N.
Instituto de Investigaciones Químicas (IIQ), Universidad Mayor de San Andrés (UMSA), Calle 27 de Cota Cota, Campus Universitario, La Paz, Bolivia.
Received: February 7, 2026; Accepted: May 7, 2026

Abstract
Aluminum modified rice husk biochar (BC-Al) was prepared as an alternative renewable adsorbent to treat fluoride contaminated drinking water. The adsorbent was characterized by Brunauer–Emmett–Teller (BET) method, point of zero charge (PZC), scanning electron microscopy (SEM–EDS) and Fourier-transform infrared spectroscopy (FTIR). Batch and column experiments were realized in order to determine the fluoride removal efficiency at different operating conditions. The results showed that BC-Al has a surface area of 39.35 m^2/g, a PZC of 4.9 and the presence of aluminum in its surface. The BC-Al removes > 90 % of the fluoride present in water, follows a pseudo second order kinetic and fits the Sips isotherm model. The maximum adsorption capacity was 5.163 mg/g, working in a pH range from 2.5 to 7.0, with an adsorbent dose of 3.33 g/l and a contact time of 9 hours. The HCO_3^- has a negative effect on fluoride removal efficiency. In column experiments, the maximum adsorption capacity was 2.997 mg/g according to the logarithmic Thomas model. It was estimated by scaling up calculations that 85.78 liters of water could be treated in a time of 6.80 hours in a column with about 1 kg of BC-Al at pilot level.
Keywords: Adsorption, aluminum, biochar, fluoride, rice husk.

Resumen
El biochar de cáscara de arroz modificado con aluminio (BC-Al) fue preparado como una alternativa de adsorbente renovable para tratar aguas contaminadas con fluoruro. El adsorbente fue caracterizado mediante el método Brunauer–Emmett–Teller (BET), punto de cero carga (PZC), microscopía electrónica de barrido (SEM – EDS) y Espectroscopia infrarroja por trasformada de Fourier (FTIR). Experimentos a nivel batch y en columna fueron realizados para determinar la eficiencia de remoción de fluoruro a distintas condiciones de operación. Los resultados muestran que el BC-Al tiene un área superficial de 39.35 m^2/g, un PZC de 4.9 y la presencia de aluminio en su superficie. El BC-Al remueve > 90 % del fluoruro presente en agua, siguiendo una cinética de pseudo segundo orden y se ajusta al modelo de isoterma de Sips. La capacidad de adsorción máxima fue de 5.163 mg/g, trabajando en un rango de pH de 2.5 a 7.0, con una dosis de adsorbente de 3.33 g/l y un tiempo de contacto de 9 horas. El HCO_3^- tiene un efecto negativo en la eficiencia de remoción de fluoruro. En las pruebas de columna, la capacidad de adsorción máxima fue de 2.997 mg/l de acuerdo al modelo logarítmico de Thomas. Se estimó mediante cálculos de escalamiento que se podrían tratar 85.78 litros de agua en un tiempo de 6.80 horas en una columna con aproximadamente 1 kg de BC-Al a nivel piloto.
Palabras clave: Adsorción, aluminio, biochar, fluoruro, cáscara de arroz.

* *Corresponding author. E-mail*: martinez.8260989@gmail.com ;
https://doi.org/10.24275/rmiq/IA26791
ISSN:1665-2738, *issn-e*: 2395-8472

1 Introduction

Fluorine ranks thirteen in terms of elemental abundance within the Earth's crust (Han *et al.*, 2021, Sivasankar *et al.*, 2012) and is released to the environment through natural causes, like weathering and mineral dissolution, and through human activities like electroplating, metal processing, the electronic manufacturing sector, the use of phosphate fertilizers, the manufacture of bricks, glass and ceramics among others (Han *et al.*, 2021).

The permissible limit of fluoride concentration in drinking water is 1.5 mg/l according to the World Health Organization (WHO). At this concentration fluorine plays a beneficial role in dental and skeletal formation, however, prolonged exposure at higher concentrations can cause dental and skeletal fluorosis (Kromah *et al.*, 2022).

Many cases of fluorosis have been reported worldwide, mainly caused by the consumption of groundwater where fluoride concentrations range between 0.1 and 20 mg/l (Kimambo *et al.*, 2019). In Bolivia, in the municipality of San Pedro, Santa Cruz, cases of dental fluorosis were reported in 80 % of the population, where fluoride concentrations in water were found to reach 6.8 mg/l (Huallpara *et al.*, 2021).

To address this problem, many defluoridation techniques had been developed like precipitation, adsorption, and ionic exchange. Adsorption is the most advantageous due to it is low cost, effective, easy to operate, has high removal capacity and the adsorbents can be regenerated and reused (He *et al.*, 2020). Currently, the most widely employed adsorbents in fluoride remediation are activated alumina, metal oxides and materials based on charcoal like biochar and activated carbon (Sha *et al.*, 2021). In this context, aluminosilicate materials such as zeolites have also shown potential for defluoridation, where both aluminum and silicon contribute to fluoride adsorption (Flores-Alamo *et al.*, 2025, Pérez-Escobedo *et al.*, 2016).

Biochar, a product derived from the thermochemical decomposition of biomass, has been used to remove different aqueous contaminants like pathogenic microorganisms, heavy metals, dyes and pesticides (Enaime *et al.*, 2020). Its efficiency is mainly due to its attractive properties such as high surface area, optimized pore size distribution and presence of surface functional groups (Enaime *et al.*, 2020). This material is gaining much attention because it is an environmentally friendly material and has a low cost of production (Xiang *et al.*, 2020).

Generally pristine biochar has limited adsorption capacity of anionic and inorganic contaminants; therefore, biochar is usually modified with metallic cations like Ca^{+2}, Fe^{+3}, Al^{+3} y La^{+3} (Liu *et al.*, 2019). Among these, aluminum has the greatest affinity for fluoride.

Although there are studies of aluminum – modified biochars that efficiently remove fluoride from water, many of these remain limited to batch systems using synthetic fluoride solutions with high fluoride concentrations (~100 mg/l); furthermore, the evaluation of these materials to continuous or pilot systems is still lacking.

Most works have used precursors such as food waste (Meilani *et al.*, 2021), corn stalk (Zhang *et al.*, 2021) or other biomass, while relatively few have studied rice husk, an agricultural residue widely available in Bolivia and Latin America countries. Rice husk is a promising material due to its high silica content that gives biochar a stable porous structure which, after chemical modifications or activations, contributes to increasing the number of active sites available for adsorption (Liu *et al.*, 2023).

Our previous work (Martínez Paredes & Lopez N., 2024) showed that rice husk is a better precursor than sugarcane bagasse (both wastes commonly found in Bolivia) for fluoride removal, and that modification with aluminum provides better performance than other modifiers tested.

Based on these results, the present study aims to evaluate the fluoride removal efficiency of aluminum - modified rice husk biochar, in batch and continuous systems, under more realistic conditions. Additionally, this work studies column design and preliminary pilot – scale upscaling.

2 Materials and methods

2.1 Materials

NaF, NaOH, HCl, KCl, K_2SO_4, KNO_3 and $NaHCO_3$ were analytical grade purchased from Scharlau, Spain. A fluoride stock solution of 1000 ppm was prepared using NaF dissolved on deionized water. The other fluoride solutions of lower concentrations were prepared by dilution with deionized water.

Rice husk was obtained from the rice producers of the municipality of Caranavi (Yungas), Department of La Paz, which was washed many times with distillated water in order to remove impurities and dried in an electrical drying oven (E28, BINDER GmbH, Germany) at 70 °C for 24 hours.

2.2 Biochar preparation

Aluminum – modified rice husk biochar (BC-Al) was obtained based on the methodology proposed by Meillani *et al.*, (2021).

Firstly, 100 g of rice husk was added into 300 ml of 0,71 M $AlCl_3$ solution for 48 hours. The mixture was dried in an electrical drying oven for 24 hours. Secondly, the sample was pyrolyzed in a horizontal tube furnace (CHY – T12100A, Henan Chengyi Equipment Science and Technology Co., China) from room temperature to 400 °C at 7 °C/min for 39 minutes and a flow rate of 100 ml/min of Argon. Finally, BC-Al was crushed to 250 μm particle size.

Pristine rice husk biochar (BC) was obtained under similar pyrolysis conditions, without the impregnation with aluminum solution.

2.3 Characterization

Specific surface area was calculated with Brunauer – Emmett – Teller (BET) method according to ASTM D6556 (ASTM International, 2014), using a chemisorption analyzer (ChemBET – TPR/TPD, Quantachrome Instruments, USA). The point of zero charge (PZC) was determined following the pH drift method (Khan & Sarwar, 2007), adding 0.5 g of adsorbent to 20 ml of 0.01 M NaCl solution, regulating initial pH with 0.1 M HCl and 0.1 M NaOH solutions and registering initial and final pH with a handheld pH meter (pH 6+, Oakton Instruments, USA).

Surface morphology of BC and BC-Al was observed using a scanning electronic microscope (TM3000, Hitachi High - Tech, Japan) and the surface elements were detected with Energy Dispersive X - ray Spectroscopy (X-Max 50, Oxford Instruments, UK).

Surface functional groups were measured by Fourier - transform infrared spectroscopy (Spectrum BX, PerkinElmer, USA) in the range of 600 and 4000 cm^{-1}, with a total of 10 scans per sample.

2.4 Batch adsorption experiments

Adsorption experiments were carried out with 30 ml of fluoride solutions using 50 ml polyethylene flasks that were put on magnetic stirrers at room temperature and 150 rpm. The effect of initial pH (2.5 – 10.0), biochar dose (0.1 – 3.33 g/l), contact time (0.5 – 30 hours), initial fluoride concentration (3 – 20 mg/l) and other co-existing ions (Cl^-, NO_3^-, SO_4^{-2}, HCO_3^-) were examined.

The pH of the solution was regulated with 0.1 M HCl and 0.1 M NaOH solutions. For each adsorption test the samples were filtered using Whatman filter paper grade 40. The residual fluoride concentration was measured using the SPADNS method (4500-F^- D) according to APHA (2017). Each test was realized in triplicate.

The fluoride removal efficiency (η) was determined by the Eq. 1:

$$\eta = \left(\frac{C_o - C_t}{C_o}\right)100\% \tag{1}$$

The adsorption capacity (q_t) was calculated by the Eq. 2:

$$q_t = \left(\frac{C_o - C_t}{m}\right) \tag{2}$$

Where C_o y C_t are the fluoride concentration (mg/l) at the beginning and at time "t" respectively, V is the volume of the solution (ml) and m is the biochar mass (mg).

For adsorption kinetic experiments, 10 mg/l fluoride solution, adjusted to pH 7.0, was treated with 3.33 g/l of adsorbent, taking samples at different contact times. The experimental data was adjusted to the pseudo first and pseudo second order kinetic models according to the Eq. 3 and Eq. 4 respectively (Sha *et al.*, 2021):

$$q_t = q_e \left(1 - \exp^{-k_1 t}\right) \tag{3}$$

$$q_t = \frac{{q_e}^2 k_2 t}{1 + k_2 q_e t} \tag{4}$$

Where q_e and q_t represent the adsorption capacities at equilibrium and at specific time "t" respectively (mg/g), k_1 (h^{-1}) is the pseudo first rate constant and k_2 (g mg^{-1} h^{-1}) is the pseudo second rate constant.

The adsorption isotherms were studied at an adsorbent dose of 3.33 g/l and at different initial fluoride concentrations (3 – 20 mg/l) for 24 hours. The experiments were realized at room temperature and a neutral pH. Experimental data was fitted to the Freundlich, Langmuir, Redlich Peterson and Sips adsorption isotherms models according to Eq. 5, Eq. 6, Eq. 7 and Eq. 8 respectively (Wang & Guo, 2020):

$$q_e = K_F {C_e}^{\frac{1}{n}} \tag{5}$$

$$q_e = \frac{q_{\max} K_L C_e}{1 + K_L C_e} \tag{6}$$

$$q_e = \frac{K_{RP} C_e}{1 + a_{RP} {C_e}^g} \tag{7}$$

$$q_e = \frac{q_{ms} K_s {C_e}^{n_s}}{1 + K_s {C_e}^{n_s}} \tag{8}$$

Where C_e is the fluoride concentration in equilibrium, K_F and n are the Freundlich constants; K_L is the Langmuir constant; $q_{\max}$ is the maximum adsorption capacity; K_{RP}, a_{RP} and g are the Redlich Peterson constants; K_s and n_s are the Sips constants and q_{ms} is the maximum amount adsorbed.

The kinetic and isotherm models were fitted to the experimental data using non-linear regression analysis. The goodness of fit of each model was evaluated using the coefficient of determination (R^2) and the root mean square error (RMSE). All analyses were performed using OriginPro 2017 software.

2.5 Adsorbent regeneration

The methodology proposed by Wang *et al.*, (2018) was used. The initial fluoride concentration and the biochar

BC-Al dose were 10 mg/l and 3.33 g/l, respectively. Fluoride- loaded biochar was washed several times with distilled water and then, was added in 50 ml of 0.1 M NaOH solution at 30 °C and 150 rpm for 3 hours. Then, the same procedure was realized using a 0.1 M solution of HCl. The previously washed biochar was dried in an electrical drying oven at 70 °C for 24 hours. Finally, the biochar was used again for adsorption tests. Four regeneration cycles were realized.

2.6 *Column adsorption experiments*

BC-Al was packed in a quartz column of 1.65 cm diameter and 40 cm length using cotton at the bottom and the surface of the column. The 10 mg/l fluoride solution entered in contact with the adsorbent in down flow. The influence of the bed height and the flow rate were studied taking samples from the exit of the column at different times in order to determinate the breakthrough curve and the breakthrough time, considering that, in the case of fluoride and according to the permissible limits established for the World Health Organization , the breakthrough time is when the effluent concentration (C_t) is 15 % of the initial concentration (C_o) (Vivek Vardhan & Srimurali, 2020).

Breakthrough curves were fitted to the Thomas model expressed in logarithmic thermals according to Eq. 9, using non-linear regression analysis and determining the coefficient of determination (R^2) and the root mean square error (RMSE). OriginPro 2017 software was used.

$$\frac{C_t}{C_o} = \frac{1}{1 + exp(k_T * \ln ln\left(\frac{q_o * M}{Q}\right) - k_T * \ln ln\,(\,C_o * t))} \quad (9)$$

k_T is the Thomas rate constant (ml/min mg), q_o is the quantity of adsorbed contaminant per unit of adsorbent mass (mg/g), M is the adsorbent mass (g) and Q is the volumetric flow (ml/min).

Only the Tomas model was used because it is mathematically equivalent to the Bohart - Adams and Yoon - Nelson models (Apiratikul & Chu, 2021), in addition to providing the adsorption capacity and the Thomas rate constant which are useful for the scaling up.

2.7 *Scaling up for column adsorption*

The height of the column at pilot level was determined according to the principle of geometric similarity (Eq. 10), using the height and the diameter of the column at laboratory level. The feed rate was determined applying the principle of kinematic similarity, using the concept of velocity correspondence (Eq. 11):

$$\frac{H_{lab}}{D_{lab}} = \frac{H_{pil}}{D_{pil}} \quad (10)$$

The feed rate was determined applying the principle of kinematic similarity, using the concept of velocity correspondence:

$$\frac{Q_{lab}}{{D_{lab}}^2} = \frac{Q_{pil}}{{D_{pil}}^2} \quad (11)$$

Where H_{lab} and H_{pil} represented the column heights at laboratory and pilot scales, Q_{lab} and Q_{pil} the corresponding flow rates, and D_{lab} and D_{pil} the column diameters at each scale.

The adsorbent mass for the column at pilot scale was determined using the Eq. 12.

$$M = \rho_{ads} * A * H \quad (12)$$

Where M is the adsorbent mass, ρ_{ads} is the adsorbent bulk density determined following the ISO 17828 methodology (ISO, 2015), A is the bedding area and H is the column height.

The operating time of the column on pilot scale "t_b" and the volume of water to be treated "V" was determined by predicting the rupture curves following the Thomas logarithm model, according to Eq. 9, using the k_T and q_o values obtained at laboratory scale.

3 Results and discussion

3.1 *Biochar characterization*

The characterization results are summarized in Table 1.

The modification with aluminum allows an increase in BC-Al specific surface area five times higher than the biochar BC. This enhancement could be due to the presence of aluminum hydrate, which is a precursor of AlOOH, that acts like an activating agent of biochar during the pyrolysis (Zhang *et al*., 2021).

The PZC of BC-Al decreases in comparison with the PZC of BC, probably due to the presence of Cl^- that reduces the PZC of alumina (Korah *et al*., 2003). This PZC value obtained suggests that the BC-Al is positively charged at a pH lower than 4.9.

According to scanning electron microscopy analysis, BC has a smooth surface with cracks and gaps in the form of slits (Figure 1a). On the other hand, BC-Al has a more porous structure and has scale–like nodules which are aluminum fixed on its surface (Figure 1b), as previously documented by Meilani *et al*., (2021).

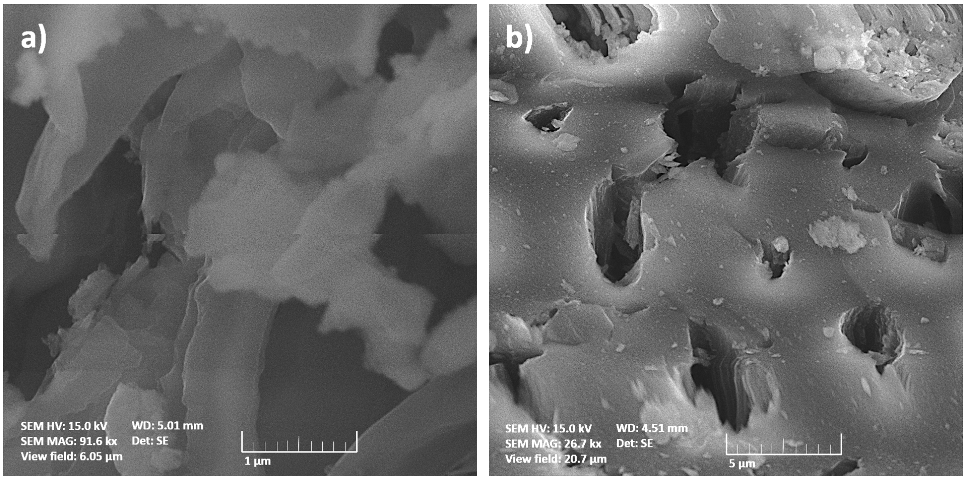

Figure 1. Scanning electron micrograph of a) BC and b) BC-Al.

Table 1. Physicochemical properties of BC and BC-Al.

Biochar	Pyrolysis yield	Surface area [m^2/g]	PZC	Surface composition [%]				
				%O	%Si	%C	%Al	%Cl
BC	45.4 %	8.5	7.6	49.7	28.6	21.6	-	-
BC-Al	46.1 %	39.3	4.9	28.3	15.5	52.7	2.6	0.7

The elements on the surface of BC and BC-Al were determined using EDS (Table 1). The presence of Si on BC is due to the high content of silicon present in rice husk. In contrast, BC-Al presents a decrease in silicon content and the presence of aluminum and chloride on its surface. The decrease in silicon can occur due to the presence of chlorine according to Eq. 13 (Gómez *et al.*, 2011).

$$SiO_{2\,(s)} + 2C_{(S)} + 2Cl_{2\,(g)} \rightarrow SiCl_{4\,(g)} + CO_{2\,(g)} \tag{13}$$

The FTIR spectra (Figure 2) shows that BC exhibited a strong Si - O - Si vibration at 1000 - 1100 cm^{-1} confirming the high silica content on rice husk biochar. Peaks were also found at 2928 and 3300 cm^{-1} which correspond to C – H and – OH vibrations respectively (Wei *et al.*, 2017). After aluminum modification (BC-Al) signals appear at 600 - 700 cm^{-1}, which are related to the Al – O bonds (Liu *et al.*, 2012), suggesting the incorporation of Al onto the biochar surface. Peaks are also observed at 1500 - 1600 cm^{-1}, corresponding to the C=C bonds. The shift of the Si – O peak from 1079 to 1102 cm^{-1} suggests that aluminum interacted with the surface groups of the silica.

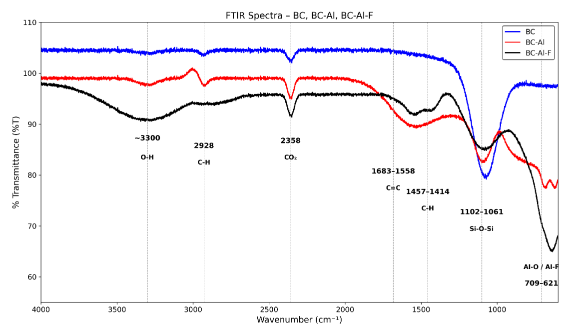

Figure 2. FTIR spectra of BC, BC-Al and BC-Al-F.

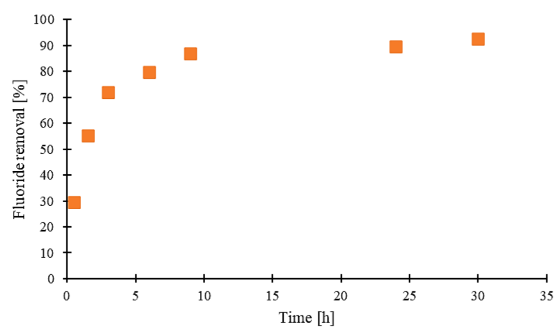

Figure 3. Influence of contact time on fluoride removal by BC-Al.

3.2 *Batch adsorption tests*

3.2.1 *Influence of contact time and adsorption kinetics*

Experiments were realized at a pH of 7.0, an adsorbent dose of 3.33 g/l and a constant rate of 150 rpm, taking samples at different intervals of time till reaching 30 hours. According to Figure 3, the maximum percentage of BC-Al fluoride removal was 92.8 % in 30 hours; however, it reaches the permissible limit in 9 hours. In the case of BC, during the first hours there is a minimal fluoride adsorption then, suddenly

Table 2. Fitting of adsorption data to kinetic equations of BC-Al.

Pseudo - first order				Pseudo - second order			
k_1 [1/h]	q_t [mg/g]	R^2	RMSE	k_2 [g/mg h]	q_t [mg/g]	R^2	RMSE
0.664	2.425	0.967	0.109	0.357	2.645	0.996	0.048

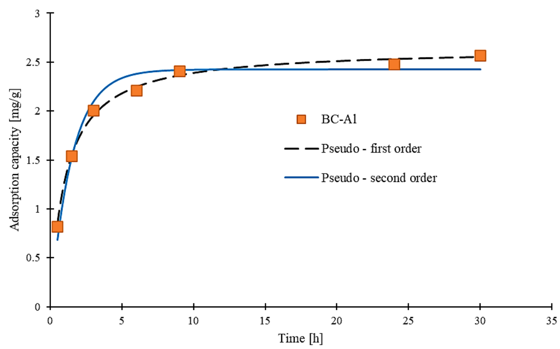

Figure 4. Kinetics of fluoride adsorption by BC-Al.

reaches its maximum point at 9 hours, adsorbing 26.9 % of fluoride and subsequently desorbing the adsorbed fluoride.

The adsorption kinetics of BC-Al was shown in Figure 4 and the values of fitting parameters are shown in Table 2. The adsorption kinetic fits better with the pseudo second order model because of the value of R^2 = 0.996 and RMSE = 0.048 obtained. Thus, the adsorption process of fluoride on BC-Al is a chemical adsorption process (Mei *et al*., 2020).

3.2.2 Influence of contact time and adsorption kinetics

Figure 5a shows the influence of adsorbent dose in the fluoride removal. Experiments were realized with 10 mg/l fluoride solution with a pH value of 7.2 at 150 rpm for 24 hours. The fluoride removal percentage increases from 26.5 % to 90.4 % when the adsorbent dose increases from 0.3 g/l to 3.33 /l because of the increase in the availability of active sites (Mei *et al*., 2020; Sadhu *et al*., 2022).

3.2.3 Influence of pH

The influence of the solution's pH was studied working at acid, neutral and basic conditions, at a fluoride concentration of 10 mg/l with an adsorbent dose of 3.33 /l at 150 rpm for 24 hours.

The fluoride removal percentage decreases as the pH increases (Figure 5b), reaching 97 % of the fluoride removal when the solution pH is 2.5 and 54.5 % when the solution pH is basic.

According to the PZC obtained, at pH lower than 4.9 the fluoride removal occurs due to the magnetic attraction between fluoride and the positive charge that BC-Al has and, a pH higher than 4.9, BC-Al has negative charge, so it repels fluoride, decreasing its percentage removal.

3.2.4 Influence of initial fluoride concentration and adsorption isotherms

The concentration range varies from 3 to 20 mg/l at pH 7.0 for 24 hours with an adsorbent dose of 3.33 g/l. Figure 6 shows that the increase in fluoride concentration reduces slightly the fluoride removal percentage from 79.3 % to 70.8 %.

Experimental data of adsorption capacity and concentration at the equilibrium was fitted to the Freundlich, Langmuir, Redlich Peterson and Sips adsorption isotherms models. The Sips isotherm model has the most suitable fit compared to the other adsorption isotherm models as it showed in the Table 3 and Figure 7 (R^2 = 0.936 and RMSE = 0.272).

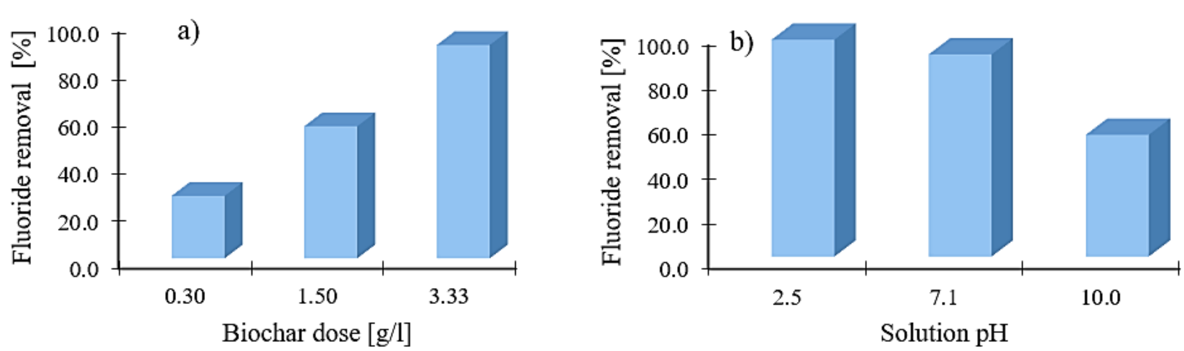

Figure 5. Influence of a) Adsorbent dose and b) Initial solution pH on fluoride removal.

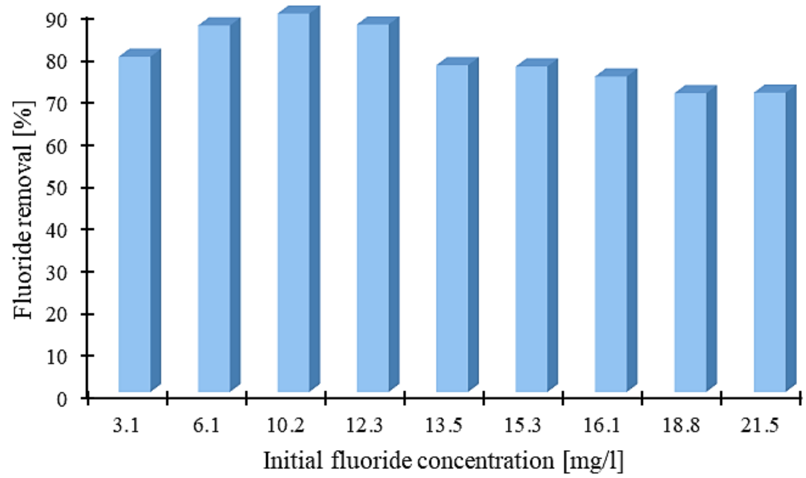

Figure 6. Influence of initial concentration on fluoride removal.

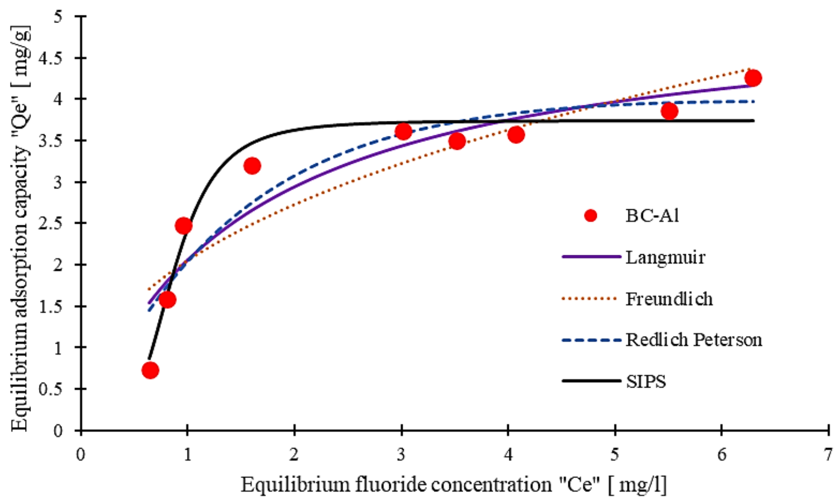

Figure 7. Fitting of biochar BC-Al to the adsorption isotherm models.

Table 3. Fitting of biochar BC-Al to the isotherm adsorption models.

Langmuir	$q_{\max}$ [mg/g]	K_L [l/mg]		R^2	RMSE
	5.163	0.660		0.856	0.440
Freundlich	K_F [$l^{1/n}$ mg$^{1-1/n}$ /g]	n		R^2	RMSE
	2.051	2.428		0.786	0.536
Redlich Peterson	K_{RP} [l/g]	α_{RP} [l/mg]	g	R^2	RMSE
	2.629	0.287	1.305	0.849	0.417
Sips	q_{ms} [mg/g]	K_S [lns/ mgns]	n_s	R^2	RMSE
	3.740	1.836	4.112	0.936	0.272

The heterogeneity parameter obtained from the Sips model (n_s = 4.112) is significantly higher than unity. This indicates that adsorption follows a Langmuir pattern, suggesting a relatively homogeneous distribution of adsorption sites and constant adsorption energy (Wang & Guo, 2020).

This result can be attributed to the modification of biochar with aluminum, which generates more uniform active sites through the formation of Al - O functional groups on biochar's surface.

Table 4. Comparison of biochar used in fluoride removal.

Raw material	Modification	Operation conditions	Adsorption capacity [mg/g]	References
Watermelon rind	-	pH = 1 Dose = 8 g/l $[F^-]$ = 5 – 100 mg/l Time = 3 h	9.5	(Sadhu *et al*., 2022)
Pine Wood	-	pH = 2 Dose = 10 g/l $[F^-]$ = 1 – 100 mg/l Time = 48 h	7.66	(Mohan *et al*., 2012)
Pine bark	-	pH = 2 Dose = 10 g/l $[F^-]$ = 1 – 100 mg/l Time = 48 h	9.77	(Mohan *et al*., 2012)
Rice husk	Nanoscale	pH = 7 Dose = 1 g/l $[F^-]$ = 3 – 10 mg/l Time = 1 h	21.7	(Goswami & Kumar, 2018)
Grape fruit peel	La^{+3}	pH = 6.5 Dose = 1 g/l $[F^-]$ = 10 – 300 mg/l Time = 9 h	19.86	(Wang *et al*., 2018)
Douglas fir	α-Fe_2O_3 y Fe_3O_4	pH = 3 Dose = 2 g/l $[F^-]$ = 1 - 60 mg/l Time = 10 min	9	(Bombuwala *et al*., 2018)
Yak dung	Fe^{+3}	pH = 5 - 6 Dose = 10 g/l $[F^-]$ = 5 - 40 mg/l Time = 24 h	4.85	(Chunhui *et al*., 2018)
Peanut Shell	MgO	pH = 8 Dose = 1 g/l $[F^-]$ = 50 mg/l Time = 400 min	83.05	(Wan *et al*., 2019)
Camellia oleifera seed shell	ZrO_2	pH = 6.8 Dose = 1.6 g/l $[F^-]$ = 10 – 30 mg/l Time = 3 h	11.04	(Mei *et al*., 2020)
Platanus acerifoli leaves	CaO	pH = 5.3 Dose = 1.6 g/l $[F^-]$ = 10 - 2000 mg/l Time = 24 h	308	(Sha *et al*., 2021)
Pinewood	$CaCl_2$	pH = 4.5 Dose = 2 g/l $[F^-]$ = 20 - 100 mg/l Time = 1 h	16.72	(Yadav *et al*., 2022)
Corn stalk	Al^{+3}	pH = 6.8 Dose = 1 g/l $[F^-]$ = 10 – 100 mg/l Time = 7 h	81.65	(Zhang *et al*., 2021)
Food waste	Al^{+3}	pH = 7.1 Dose = 3.33 g/l $[F^-]$ = 10 - 900 mg/l Time = 24 h	123.4	(Meilani *et al*., 2021)
Rice husk	Al^{+3}	pH = 7 Dose = 3.33 g/l $[F^-]$ = 3 – 21.5 mg/l Time = 24 h	5.16	This study

The maximum adsorption capacity is 5.163 mg/g for biochar BC-Al, although it is lower than the values reported in bibliography (Table 4), the material has the potential to be used in defluoridation in ranges commonly found in groundwater, where the fluoride concentration is lower than 10 mg/l.

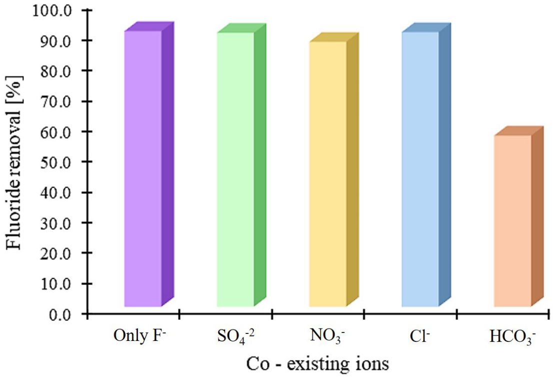

Figure 8. Influence of interferent ions on fluoride removal.

3.2.5 *Adsorption mechanism*

The structural, textural and morphological properties of BC-Al are important in its fluoride adsorption capacity. As shown in Table 1, the increase in specific surface area provides a greater number of available adsorption sites. SEM-EDS and FTIR analysis confirm the fixation of aluminum on the biochar's surface. Aluminum plays an important role in fluoride adsorption, supported by the FTIR of BC-Al after fluoride adsorption (BC–Al–F).

The FTIR of BC-Al-F (Figure 2) exhibits a shift from 1102 to 1041 cm^{-1} which indicates an interaction of fluoride with silica or aluminum species. More intense bands are also visible in 600 – 800 cm^{-1} which refer to changes in Al – O vibrations and possible formation of Al – F (Vasudevan *et al*., 2011).

Based on this, fluoride is adsorbed onto the BC-Al surface through ligand exchange, following the Eq 13 (Meilani *et al*., 2020).

$$Al - OH + F^{-} \rightarrow Al - F + OH^{-} \tag{14}$$

In the case of carrying out the adsorption process at pH lower than the PZC (4.9) the adsorption is also caused by electrostatic attraction, according to Eq. 14 (Sujana *et al*., 2009).

$$Al - OH_2{}^{+} + F^{-} \rightarrow Al - F + H_2O \tag{15}$$

3.2.6 *Influence of co – existing ions*

The influence of HCO_3^-, Cl^-, NO_3^- and SO_4^{-2} on fluoride removal has been studied. The initial fluoride concentration was 10 mg/l and the concentration of each interfering ion was 100 mg/l. The solution pH was 7.0, the biochar dose was 3.33 g/l and the contact time was 24 hours.

The HCO_3^- has the most negative effect, reducing the removal percentage of fluoride from 90.4 % to 56.1 %, this is because of the increasing on the pH and the competition between fluoride and OH^- and HCO_3^- ions (Sha *et al*., 2021; Wang *et al*., 2018). The other ions have no significant influence on fluoride removal (Figure 8).

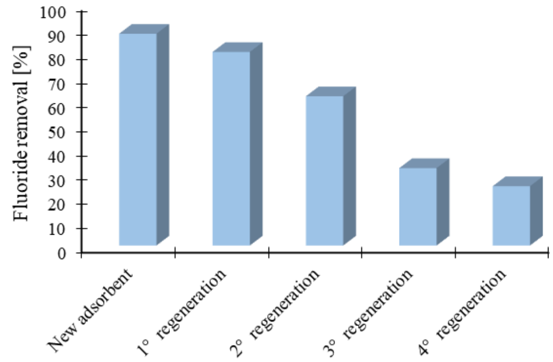

Figure 9. Biochar BC-Al regeneration test.

3.2.7 *Adsorbent regeneration*

The fluoride percentage of removal reduces from 87.6 % (initial use) to 24.5 % (fourth regeneration cycle) as can be seen in Figure 9. The biochar BC-Al still works after one regeneration cycle (80 % of fluoride removal), after that, the fluoride removal does not achieve the permissible limit established by WHO.

This behavior may be due to the formation of relatively strong Al - F bonds resulting from ligand exchange between fluoride and Al - O groups present on the BC -Al surface, limiting regeneration efficiency.

3.2.8 *Biochar applied in water samples that simulate real conditions*

Synthetic solutions with characteristics similar to San Pedro – Santa Cruz municipality were prepared, according to Huallpara *et al*., (2021).

Due to the negative effect of bicarbonate on fluoride removal, tests were carried at a solution pH of 4.7, the adsorbent dose of 3.33 g/l and the contact time of 24 hours.

The fluoride removal percentage achieved was 90.3 %, reaching a fluoride concentration of 0.6 mg/l that complies with the permissible limits.

3.3 *Column adsorption studies*

3.3.1 *Influence of bed height*

The influence of bed height on fluoride removal was studied at 13.50 and 28.50 cm, the initial fluoride concentration was 10 mg/l and the flow rate was 2.16 ml/min. The breakthrough curve was determined by plotting C_t/C_o against time.

Figure 10 shows that the increase in the bed height causes an increase in the breakthrough time from 400 to 560 min, this is because of the increase on the available active sites of the biochar.

Table 5. Fitting the breakthrough curves to the logarithmic Thomas model.

Q [ml/min]	H [cm]	Breakthrough time [min]	Volume [ml]	Adsorption capacity [mg/g]	k_T [ml/mg min]	R^2	RMSE
2.16	13.50	400	868.82	1.934	1.625	0,960	0.061
2.16	28.50	560	1197.59	2.997	1.412	0,976	0.040
10.65	13.50	5	53.46	0.584	1.319	0,966	0.048
10.65	28.50	120	1272.81	1.707	1.781	0,955	0.061

Table 6. Scaling up to pilot scale to different operating conditions.

	H_{pil} [cm]	M [g]	Q_{pil} [ml/min]	t_b [h]	V [l]
H_1-Q_1	60.10	473.48	42.72	16.20	41.84
H_2-Q_1	126.89	999.58	42.72	45.78	116.47
H_1-Q_2	60.10	473.48	211.11	0.77	9.75
H_2-Q_2	126.89	999.58	211.11	6.80	85.78

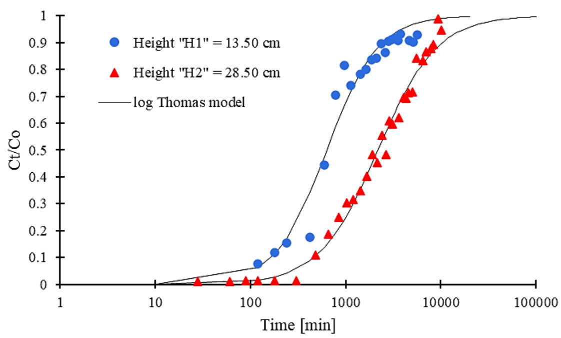

Figure 10. Influence of bed height on breakthrough curves.

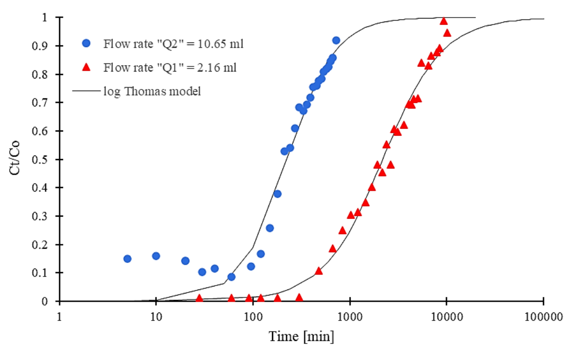

Figure 11. Influence of flow rate on breakthrough curves.

3.3.2 *Influence of flow rate*

The influence of bed height was studied at 2.16 and 10.65 ml/min, with an initial fluoride concentration of 10 mg/l and a bed height of 28.50 cm. Figure 11 shows that the increase in the flow rate reduces breakthrough time from 400 to 120 minutes. This is mainly due to the decrease in contact time between the adsorbent and the adsorbate, which causes intra-particle diffusion to become less effective. At a higher flow rate, the adsorbent becomes saturated more quickly due to a weak distribution of the liquid in the column.

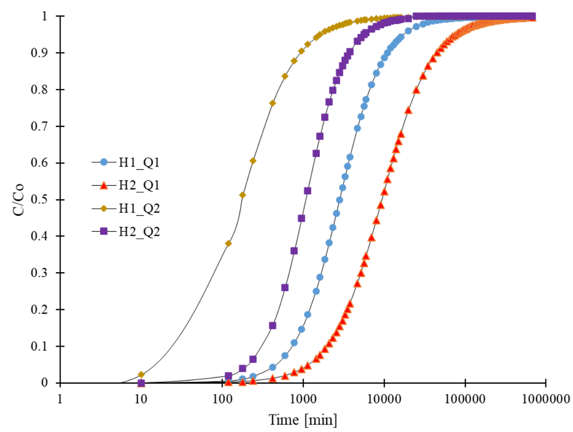

Figure 12. Predicted breakthrough curves at pilot scale.

3.3.3 *Fitting of breakthrough model curves*

Table 5 shows that data fit well to the logarithmic Thomas model having R^2 values higher than 0.95 and RMSE values lower than 0.061. The maximum adsorption capacity is 2.997 mg/g at the maximum height (H_2 = 28.50 cm) and the lowest flow rate (Q_1 = 2.16 ml/min), which corresponds to a higher breakthrough time (560 min) and therefore a greater volume of water to be treated (1197.59 ml).

3.3.4 *Scaling up*

Table 6 exhibits the results for the column at pilot level. A nominal diameter of 3 inches was considered for the column at pilot level and the bulk density of BC-Al was 0.119 g/ml.

The breakthrough curves at pilot level were found in Figure 12.

The better operating conditions were found at the maximum height "H_2" and the highest flow rate "Q_2" which corresponds to 28.50 cm and 10.65 ml/min in laboratory scale. It is equivalent to 126.89 cm and 211.11 ml/min in pilot scale. At that operating conditions 85.78 liters of water could be treated in 6.80 hours. Considering this, the dimensions of a pilot

Table 7. Dimension of the column at laboratory and pilot level.

	Laboratory scale	Pilot scale
Geometric parameters		
Internal diameter [cm]	1.65	7.35
Area [cm^2]	2.14	42.38
Column height [cm]	34.00	151.45
Operational parameters		
Linear velocity [cm/min]	4.96	4.96
Flow rate [ml/min]	10.65	211.11
Bed height [cm]	28.50	126.89
Adsorbent mass [g]	10.66	999.58

level column for treating fluoride contaminated water are shown in Table 7.

Conclusions

The aluminum modified rice husk biochar (BC-Al) effectively reduces fluoride concentrations to levels below permissible limits in a pH range that goes from 2.5 to 7.0, with an adsorbent dose of 3.33 g/l, reaching the equilibrium in 9 hours. The biochar BC-Al follows pseudo second order kinetics, fitting to the Sips isotherm in batch tests and the Thomas logarithmic model in continuous column systems.

The good performance of BC-Al is related to its physicochemical properties. Aluminum modification increased the specific surface area from 8.5 m^2/g to 39.3 m^2/g, shifted the PZC to 4.9 (favoring electrostatic attraction at pH lower than this) and generated a rougher morphology with well-dispersed aluminum sites, making ligand exchange the main adsorption mechanism. These changes provided more active sites and good selectivity.

Although BC – Al exhibits a modest adsorption capacity (5.163 mg/g and 2.997 mg/g at batch and continuous systems respectively), it offers significant advantages compared to many high – capacity laboratory adsorbents.

Unlike other materials that suffer a decrease in defluoridation efficiency, mainly due to strong competition from coexisting anions (particularly bicarbonates) and mass transfer limitations at lower fluoride concentrations, BC – Al maintained high removal efficiencies (> 90 %) in simulated groundwater, despite the presence of bicarbonates, adjusting pH at 4.7, being feasible in batch and continuous systems.

BC-Al can be regenerated for one cycle, after which its efficiency declines due to strong bonds formed by ligand exchange, however this contributes to its good selectivity.

Scaling up shows that 1 kg of BC – Al can treat 85.78 liters of water in 6.80 hours, being acceptable for decentralized systems such as household or small community filters where rice husks are generated in large quantities making it a sustainable and low-cost adsorbent.

Overall, BC-Al is a promising material for defluoridation, as it effectively treats water with similar characteristics to those found in real groundwater, combining adequate performance, resistance to interfering ions, low cost and ease of implementation.

Acknowledgements

This work was supported by the Swedish International Development Cooperation Agency (SIDA), Swiss Agency for Development and Cooperation (COSUDE) and The World Academy of Sciences (TWAS).

References

American Public Health Association. (2017). 4500-F-D. SPADNS Method. In: *Standard Methods for the Examination of Water and Wastewater* (23rd ed.). APHA Press, USA.

Apiratikul, R., & Chu, K. H. (2021). Improved fixed bed models for correlating asymmetric adsorption breakthrough curves. *Journal of Water Process Engineering, 40*, 101810. https://doi.org/10.1016/j.jwpe.2020.101810

ASTM International. (2014). *ASTM D6556-14: Standard Test Method for Carbon Black - Total and External Surface Area by Nitrogen Adsorption*. astm.org

Bombuwala, N., Liyanage, A. S., Pittman, C. U., Mohan, D., & Mlsna, T. (2018). Fast nitrate and fluoride adsorption and magnetic separation from water on α -Fe_2O_3 and Fe_3O_4 dispersed on Douglas fir biochar. *Bioresource Technology*, *263*(April), 258–265. https://doi.org/10.1016/j.biortech.2018.05.001

Chunhui, L., Jin, T., Puli, Z., Bin, Z., Duo, B., & Xuebin, L. (2018). Simultaneous removal of fluoride and arsenic in geothermal water in Tibet using modified yak dung biochar as an adsorbent. *Royal Society Open Science*, *5*(11), 181266. https://doi.org/10.1098/rsos.181266

Enaime, G., Baçaoui, A., Yaacoubi, A., & Lübken, M. (2020). Biochar for wastewater treatment-conversion technologies and applications. *Applied Sciences*, *10*(10), 3492. https://doi.org/10.3390/app10103492

Flores-Alamo, N., Vásquez-Méndez J.I., Solache-Rios, M.J., Cuellar-Robles, F., & Carreño-de-León, M.C. (2025). Removal of fluoride ions from aqueous solutions and water for human consumption by a surfactant modified zeolite. Revista Mexicana de Ingeniería Química, 24(2), IA25491. https://doi.org/10.24275/rmiq/IA25491

Goswami, R., & Kumar, M. (2018). Removal of fluoride from aqueous solution using nanoscale rice husk biochar. *Groundwater for Sustainable Development 7*, 446–451. https://doi.org/10.1016/j.gsd.2017.12.010

Han, J., Kiss, L., Mei, H., Remete, A. M., Ponikvar-Svet, M., Sedgwick, D. M., Roman, R., Fustero, S., Moriwaki, H., & Soloshonok, V. A. (2021). Chemical Aspects of Human and Environmental Overload with Fluorine. *Chemical Reviews*, *121*(8), 4678–4742. https://doi.org/10.1021/acs.chemrev.0c01263

He, J., Yang, Y., Wu, Z., Xie, C., Zhang, K., Kong, L., & Liu, J. (2020). Review of fluoride removal from water environment by adsorption. *Journal of Environmental Chemical Engineering*, *8*(6), 104516. https://doi.org/10.1016/j.jece.2020.104516

Huallpara, L., Ormachea, M., Escalera, R., Ormachea, O., García, J. L., Suso, J., García, M. E., Hornero, J., Pérez, F., & Robles, V. (2021). Hidroquímica De Aguas Subterráneas En El Municipio De San Pedro, Santa Cruz, Bolivia: Determinación De Fluoruro. *Revista Boliviana de Química*, *38*(1), 46–55. https://doi.org/10.34098/2078-3949.38.1.5

International Organization for Standardization. (2015). *ISO 17828: Solid biofuels—Determination of bulk density*. iso.org

Khan, M. N., & Sarwar, A. (2007). Determination of points of zero charge of natural and treated adsorbents. *Surface Review and Letters*, *14*(3), 461–469. https://doi.org/10.1142/S0218625X07009517

Kimambo, V., Bhattacharya, P., Mtalo, F., Mtamba, J., & Ahmad, A. (2019). Fluoride occurrence in groundwater systems at global scale and status of defluoridation – State of the art. *Groundwater for Sustainable Development*, *9*, 100223. https://doi.org/10.1016/j.gsd.2019.100223

Korah, J., Spieker, W. A., & Regalbuto, J. R. (2003). Why Ion-Doped, PZC-Altered Silica and Alumina Fail to Influence Platinum Adsorption. *Catalysis Letters*, *85*(1–2), 123–127. https://doi.org/10.1023/A:1022189312386

Kromah, V., Powoe, S. P. B., & Asumana, C. (2022). Groundwater Defluoridation with Composite Oxyhydroxide Mineral Ores—The Case with Bauxite, a Systematic Review. *Water, 14*(18), 2829. https://doi.org/10.3390/w14182829

Liu, C., Shih, K., Gao, Y., Li, F., &Wei, L. (2012). Dechlorinating transformation of propachlor through nucleophilic substitution by dithionite on the surface of alumina. *Journal of Soils and Sediments, 12*(5), 724–733. https://doi.org/10.1007/s11368-012-0506-0

Liu, L., Yang, X., Ahmad, S., Li, X., Ri, C., Tang, J., Ellam, R. M., & Song, Z. (2023). Silicon (Si) modification of biochars from different Si-bearing precursors improves cadmium remediation. *Chemical Engineering Journal, 457*, 141194. https://doi.org/10.1016/j.cej.2022.141194

Liu, X., Shen, F., & Qi, X. (2019). Adsorption recovery of phosphate from aqueous solution by CaO-biochar composites prepared from eggshell and rice straw. *Science of the Total Environment*, *666*, 694–702. https://doi.org/10.1016/j.scitotenv.2019.02.227

Martínez Paredes, G.X & Lopez N., L. (2024). Evaluación de la remoción de fluoruro en aguas con biochar en Bolivia. *Revista Boliviana de Química. 41*(3), 148-154. https://doi.org/10.34098/2078-3949.41.3.3

Mei, L., Qiao, H., Ke, F., Peng, C., Hou, R., Wan, X., & Cai, H. (2020). One-step synthesis of zirconium dioxide-biochar derived from *Camellia oleifera* seed shell with enhanced removal capacity for fluoride from water. *Applied Surface Science*, *509*, 144685. https://doi.org/10.1016/j.apsusc.2019.144685

Meilani, V., Lee, J. I., Kang, J. K., Lee, C. G., Jeong, S., & Park, S. J. (2021). Application of aluminum-modified food waste biochar as adsorbent of fluoride in aqueous solutions and optimization of production using response surface methodology. In *Microporous and Mesoporous Materials*, *312*, 110764. https://doi.org/10.1016/j.micromeso.2020.110764

Mohan, D., Sharma, R., Singh, V. K., Steele, P., & Pittman, C. U. (2012). Fluoride Removal from Water using Bio-Char, a Green Waste, Low-Cost Adsorbent: Equilibrium Uptake and Sorption Dynamics Modeling. *Industrial & Engineering Chemistry Research, 51*(2), 900–914. https://doi.org/10.1021/ie202189

Pérez-Escobedo, A., Díaz-Flores, P.E., Rengel-Méndez, J.R., Cerino-Córdova, F.J., Ovando-Medina, V.M., & Alcalá-Jáuregui, J.A. (2016). Fluoride adsorption capacity of composites based on chitosan-zeolite-algae. *Revista Mexicana de Ingeniería Química, 15*(1), 139-147. https://www.scielo.org.mx/pdf/rmiq/v15n1/1665-2738-rmiq-15-01-00139.pdf

Sadhu, M., Bhattacharya, P., Vithanage, M., & Padmaja Sudhakar, P. (2022). Adsorptive removal of fluoride using biochar – A potential application in drinking water treatment. *Separation and Purification Technology*, *278*, 119106. https://doi.org/10.1016/j.seppur.2021.119106

Segura Gómez, E., Álvarez Guzman, G., Gutiérrez Fuentes J. A., Martínez Rosales J. M., & Cervantes Jáuregui J. A. (2011). Influencia de las propiedades superficiales en reacciones de halogenación de sílice de origen biogénico. *Acta Universitaria*, *21*(4), 55 – 64. https://doi.org/10.15174/au.2011.31

Sha, Q., Xie, H., Liu, W., Yang, D., He, Y., Yang, C., Wang, N., & Ge, C. (2021). Removal of fluoride using platanus acerifoli leaves biochar–an efficient and low-cost application in wastewater treatment. *Environmental Technology, 44*(1), 93-107. https://doi.org/10.1080/09593330.2021.1964002

Sivasankar, V., Rajkumar, S., Murugesh, S., & Darchen, A. (2012). Tamarind (*Tamarindus indica*) fruit shell carbon: A calcium-rich promising adsorbent for fluoride removal from groundwater. *Journal of Hazardous Materials*, *225–226*, 164–172. https://doi.org/10.1016/j.jhazmat.2012.05.015

Sujana, M.G., Soma G., Vasumathi, N., & Anand, S. (2009). Studies on fluoride adsorption capacities of amorphous Fe/Al mixed hydroxides from aqueous solutions. *Journal of Fluorine Chemistry, 130*(8), 749–754. https://doi.org/10.1016/j.jfluchem.2009.06.005

Vasudevan, S., Kannan, B. S., Lakshmi, J., Mohanraj, S., & Sozhan, G. (2011). Effects of alternating and direct current in electrocoagulation process on the removal of fluoride from water. *Journal of Chemical Technology and Biotechnology, 86*(3), 428–436. https://doi.org/10.1002/jctb.2534

Vivek Vardhan, C. M., & Srimurali, M. (2020). Development of a low-cost column type filter based on agricultural waste for removal of fluoride from water. In: *Recent trends in waste water treatment and water resource management*, (S. K. Ghosh, ed), Pp. 111–118. Springer, Singapore

Wan, S., Lin, J., Tao, W., Yang, Y., Li, Y., & He, F. (2019). Enhanced Fluoride Removal from Water by Nanoporous Biochar-Supported Magnesium Oxide. *Industrial & Engineering Chemistry Research*, *58*(23), 9988–9996. https://doi.org/10.1021/acs.iecr.9b01368

Wang, J., Chen, N., Feng, C., & Li, M. (2018). Performance and mechanism of fluoride adsorption from groundwater by lanthanum-modified pomelo peel biochar. *Environmental Science and Pollution Research*, *25*, 15326–15335. https://doi.org/10.1007/s11356-018-1727-6

Wang, J., & Guo, X. (2020). Adsorption isotherm models: Classification, physical meaning, application and solving method. *Chemosphere*, *258*, 127279. https://doi.org/10.1016/j.chemosphere.2020.127279

Wei, L., Huang, Y., Li, Y., Huang, L., Mar, N. N., Huang, Q., & Liu, Z. (2017). Biochar characteristics produced from rice husks and their sorption properties for the acetanilide herbicide metolachlor. *Environmental Science and Pollution Research, 24*(5), 4552–4561. https://doi.org/10.1007/s11356-016-8192-x

Xiang, W., Zhang, X., Chen, J., Zou, W., He, F., Hu, X., Tsang, D. C. W., Ok, Y. S., & Gao, B. (2020). Biochar technology in wastewater treatment: A critical review. *Chemosphere*, *252*, 126539. https://doi.org/10.1016/j.chemosphere.2020.126539

Yadav, T. K., Abhishek, Prasad, B., Singh, D., & Prasad, K. S. (2022). Calcium Pretreated *Pinus Roxburghii* Wood Biochar for Adsorptive Removal of Fluoride from Aqueous Solution. *Biointerface Research in Applied Chemistry*, *12*(4), 4307–4316. https://doi.org/10.33263/BRIAC124.43074316

Zhang, X., Qi, Y., Chen, Z., Song, N., Li, X., Ren, D., & Zhang, S. (2021). Evaluation of fluoride and cadmium adsorption modification of corn stalk by aluminum trichloride. *Applied Surface Science*, *543*, 148727. https://doi.org/10.1016/j.apsusc.2020.148727